

# New Donor- $\pi$ -Acceptor Type Triazatruxene Derivatives for Highly Efficient Dye-Sensitized Solar Cells

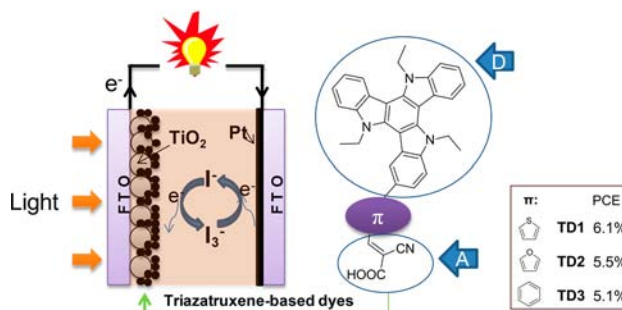
Xing Qian,<sup>†</sup> Yi-Zhou Zhu,<sup>\*,†</sup> Jian Song,<sup>‡</sup> Xue-Ping Gao,<sup>‡</sup> and Jian-Yu Zheng<sup>\*,†</sup>

State Key Laboratory and Institute of Elemento-Organic Chemistry, Nankai University, Tianjin, 300071, China, and Institute of New Energy Material Chemistry, Nankai University, Tianjin, 300071, China

zhuyizhou@nankai.edu.cn; jy Zheng@nankai.edu.cn

Received October 10, 2013

## ABSTRACT



A new class of organic dyes based on triazatruxene have been designed and synthesized for dye-sensitized solar cells. The photoelectronic properties of these donor- $\pi$ -acceptor dyes can be tuned by changing  $\pi$ -conjugated linkers. The best performance was found for triazatruxene dye TD1, wherein, with thiophene as the conjugated linker and cyanoacrylic acid as the acceptor, a power conversion efficiency up to 6.10% was achieved.

Dye-sensitized solar cells (DSSCs) have been considerably developed due to their significant potential to be used as low-cost devices for solar energy-to-electricity conversion.<sup>1</sup> Great efforts in many aspects covering semiconductors, counter electrodes, electrolytes, and sensitizers have been devoted to improving the power conversion efficiency.<sup>2</sup> In these cells, the sensitizers play a key role in their performance and remain one of the most studied areas.<sup>3</sup> Many new sensitizers have been reported, and currently there are two major categories of sensitizers: metal–organic complexes and metal-free organic dyes.<sup>4</sup> The metal–organic

complexes mainly include polypyridyl Ru(II) complexes, porphyrins and phthalocyanines, which have shown promising performance.<sup>5</sup> However, some problems such as toxicity, limited resource, and high cost inevitably coexist. On the other hand, metal-free organic sensitizers have attracted considerable attention for their structural diversity, high molar extinction coefficient, ease of structural tuning, and low cost.<sup>6</sup>

Triazatruxene (TAT), in which three indole units are combined by one benzene ring, can be considered as an extended delocalized  $\pi$ -system. The replacement of 5,10,15-C atoms of truxene by three N atoms endows the resultant triazatruxene with excellent electron-donating

<sup>†</sup> State Key Laboratory and Institute of Elemento-Organic Chemistry.

<sup>‡</sup> Institute of New Energy Material Chemistry.

(1) (a) O'Regan, B.; Grätzel, M. *Nature* **1991**, 353, 737. (b) Grätzel, M. *Nature* **2001**, 414, 338. (c) Grätzel, M. *Acc. Chem. Res.* **2009**, 42, 1788. (d) Yella, A.; Lee, H.-W.; Tsao, H. N.; Yi, C.; Chandiran, A. K.; Nazeeruddin, M. K.; Diau, E. W.-G.; Yeh, C.-Y.; Zakeeruddin, S. M.; Grätzel, M. *Science* **2011**, 334, 629.

(2) Hagfeldt, A.; Boschloo, G.; Sun, L.; Kloo, L.; Pettersson, H. *Chem. Rev.* **2010**, 110, 6595.

(3) (a) Clifford, J. N.; Martinez-Ferrero, E.; Viterisi, A.; Palomares, E. *Chem. Soc. Rev.* **2011**, 40, 1635. (b) Li, J.-Y.; Chen, C.-Y.; Ho, W.-C.; Chen, S.-H.; Wu, C.-G. *Org. Lett.* **2012**, 14, 5420.

(4) Do, K.; Kim, D.; Cho, N.; Paek, S.; Song, K.; Ko, J. *Org. Lett.* **2012**, 14, 222.

(5) Li, H.; Koh, T. M.; Hagfeldt, A.; Grätzel, M.; Mhaisalkar, S. G.; Grimsdale, A. C. *Chem. Commun.* **2013**, 49, 2409.

(6) (a) Kumar, D.; Thomas, K. R. J.; Lee, C.-P.; Ho, K.-C. *Org. Lett.* **2011**, 13, 2622. (b) Liang, M.; Chen, J. *Chem. Soc. Rev.* **2013**, 42, 3453. (c) Cai, S.; Hu, X.; Zhang, Z.; Su, J.; Li, X.; Islam, A.; Han, L.; Tian, H. *J. Mater. Chem. A* **2013**, 1, 4763. (d) Wang, Z.; Liang, M.; Wang, L.; Hao, Y.; Wang, C.; Sun, Z.; Xue, S. *Chem. Commun.* **2013**, 49, 5748.

(7) Robertson, N.; Parsons, S.; MacLean, E. J.; Coxall, R. A.; Mount, A. R. *J. Mater. Chem.* **2000**, 10, 2043.

(8) Ji, L.; Fang, Q.; Yuan, M.-S.; Liu, Z.-Q.; Shen, Y.-X.; Chen, H.-F. *Org. Lett.* **2010**, 12, 5192.

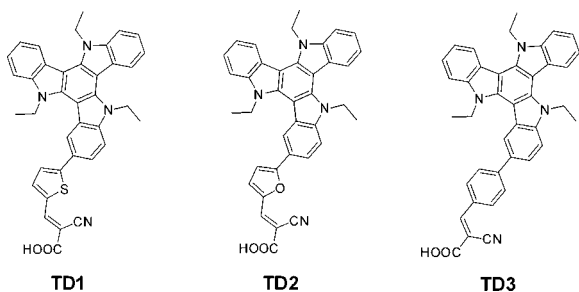
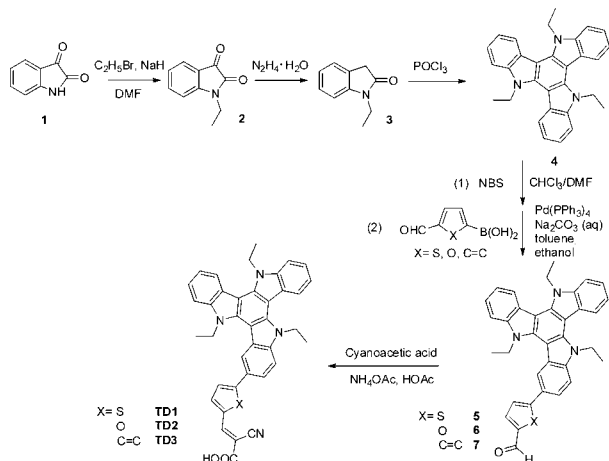


**Figure 1.** Structures of the triazatruxene-based dyes **TD1–3**.

potential for intramolecular charge transfer.<sup>7,8</sup> Owing to its unique discotic  $\pi$ -extended and electron-rich aromatic structure, this  $C_3$  symmetric fused indole trimer has been widely used to produce electroactive discotic liquid-crystalline materials,<sup>9</sup> hole transporting materials with high hole mobility,<sup>10</sup> organic-light-emitting diodes (OLEDs),<sup>11</sup> and two-photon absorption (TPA) materials.<sup>8,12</sup> However, to the best of our knowledge, there are no reports about the application in dye-sensitized solar cells. Inspired by its proven strong intramolecular charge transfer characteristic, synthetic flexibility, and high stability, we report herein the design, synthesis, and characterization of a series of new organic sensitizers based on triazatruxene.

**Scheme 1.** Synthetic Procedures of **TD1–3**



The donor- $\pi$ -acceptor (D- $\pi$ -A) structure has been commonly involved in most organic dyes owing to its efficient intramolecular charge transfer (ICT) characteristic, which is important for light harvesting.<sup>13</sup> The excited state generated by an ICT transition from donor to acceptor is responsible for the injection into the conduction band of the semiconductors.<sup>14</sup> Recently, the D- $\pi$ -A type carbazole

derivatives have been used to improve the power conversion efficiency of DSSCs and significant improvements have been achieved.<sup>13c–e</sup> Triazatruxene in which three carbazole units share one benzene ring, compared to a single carbazole system, has an enlarged  $\pi$ -system and may therefore increase the electron donating ability of the D- $\pi$ -A type dye.<sup>12</sup> So we present the D- $\pi$ -A type dyes consisting of a triazatruxene moiety acting as the electron donor and 2-cyanoacetic acid acting as the electron acceptor/anchoring group. Aromatic rings such as thiophene, furan, and benzene have been selected to act as the  $\pi$ -conjugated linkers and resulted in sensitizers **TD1**, **TD2**, and **TD3**, respectively. The molecular structures of these dyes are shown in Figure 1. The syntheses of these dyes involved two major steps: (1) Suzuki cross-coupling of brominated triazatruxene and substituted aromatic aldehydes produced the  $\pi$ -extended triazatruxene bearing aldehydes; (2) Knoevenagel reaction of the resulting aldehydes and cyanoacetic acid afforded the target sensitizers **TD1–3**. Details of the synthesis are shown in Scheme 1.

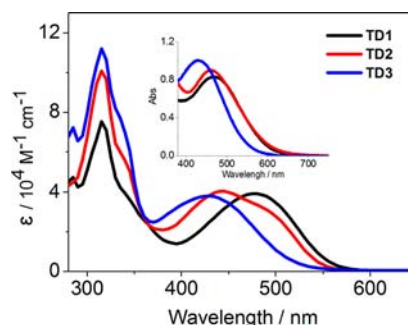


**Figure 2.** UV-vis absorption spectra of **TD1–3** in THF and on  $\text{TiO}_2$  films (inset).

The UV-vis absorption spectra of **TD1–3** are depicted in Figure 2. The data for the absorption, electrochemical properties, and frontier orbital energy levels are summarized in Table 1. Each of these organic dyes exhibits two major absorption bands at 280–350 and 400–550 nm in THF solution. The short wavelength bands can be assigned to the localized aromatic  $\pi$ - $\pi^*$  transitions, while

(9) (a) Gómez-Lor, B.; Alonso, B.; Omenat, A.; Serrano, J. L. *Chem. Commun.* **2006**, 5012. (b) Luo, J.; Zhao, B.; Shao, J.; Lim, K. A.; Chan, H. S. O.; Chi, C. *J. Mater. Chem.* **2009**, *19*, 8327. (c) Zhao, B.; Liu, B.; Png, R. Q.; Zhang, K.; Lim, K. A.; Luo, J.; Shao, J.; Ho, P. K. H.; Chi, C.; Wu, J. *Chem. Mater.* **2010**, *22*, 435.

(10) (a) Talarico, M.; Termine, R.; García-Frutos, E. M.; Omenat, A.; Serrano, J. L.; Gómez-Lor, B.; Golemme, A. *Chem. Mater.* **2008**, *20*, 6589. (b) García-Frutos, E. M.; Gutierrez-Puebla, E.; Monge, M. A.; Ramírez, R.; de Andrés, P.; de Andrés, A.; Ramírez, R.; Gómez-Lor, B. *Org. Electron.* **2009**, *10*, 643.

(11) (a) Lai, W.-Y.; Zhu, R.; Fan, Q.-L.; Hou, L.-T.; Cao, Y.; Huang, W. *Macromolecules* **2006**, *39*, 3707. (b) Lai, W.-Y.; He, Q.-Y.; Zhu, R.; Chen, Q.-Q.; Huang, W. *Adv. Funct. Mater.* **2008**, *18*, 265.

(12) Shao, J.; Guan, Z.; Yan, Y.; Jiao, C.; Xu, Q.-H.; Chi, C. *J. Org. Chem.* **2011**, *76*, 780.

(13) (a) Yan, K.; Lu, X.; Qiu, Y.; Liu, Z.; Sun, J.; Yan, F.; Guo, W.; Yang, S. *Org. Lett.* **2012**, *14*, 2214. (b) Tingare, Y. S.; Shen, M.-T.; Su, C.; Ho, S.-Y.; Tsai, S.-H.; Chen, B.-R. *Org. Lett.* **2013**, *15*, 4292. (c) Koumura, N.; Wang, Z.-S.; Mori, S.; Miyashita, M.; Suzuki, E.; Hara, K. *J. Am. Chem. Soc.* **2006**, *128*, 14256. (d) Baheti, A.; Thomas, K. R. J.; Lee, C.-P.; Ho, K.-C. *Chem.-Asian J.* **2012**, *7*, 2942. (e) Venkateswararao, A.; Thomas, K. R. J.; Lee, C.-P.; Ho, K.-C. *Tetrahedron Lett.* **2013**, *54*, 3985.

(14) Labat, F.; Bahers, T. L.; Ciofini, I.; Adamo, C. *Acc. Chem. Res.* **2012**, *45*, 1268.

the long wavelength ones correspond to intramolecular charge transfer (ICT) transitions.<sup>15</sup> The intensity of  $\pi-\pi^*$  transitions is higher than that of the ICT transitions. The absorption maxima ( $\lambda_{\text{max}}$ ) of **TD1** (476 nm) and **TD2** (442 nm) at the long wavelength region are more red-shifted in comparison to that of **TD3** (422 nm). That can be ascribed to the better electron delocalization over the whole molecule with electron-rich thiophene or furan as the conjugated linker. As shown in Figure 2, when anchoring on mesoporous TiO<sub>2</sub> films, these dyes all show significantly broadened and red-shifted absorption spectra compared with that measured in THF solutions.

**Table 1.** Photophysical, Electrochemical Data for **TD1–3**<sup>a</sup>

dye	$\lambda_{\text{max}}$ / nm	$\epsilon$ / M <sup>-1</sup> cm <sup>-1</sup>	$E_{\text{ox}}$ / V	$E_{0-0}$ / V	$E_{\text{red}}$ / V	HOMO/ LUMO/eV
<b>TD1</b>	318 476	75 336 39 319	0.91	2.03	-1.12	-5.41/-3.38
<b>TD2</b>	316 442	100 937 40 459	0.90	2.07	-1.17	-5.40/-3.33
<b>TD3</b>	317 422	112 046 38 102	0.93	2.13	-1.20	-5.43/-3.30

<sup>a</sup>  $E_{0-0}$  values (zeroth-zeroth transition energies) were estimated from the onset absorption wavelength in THF.  $E_{\text{red}} = E_{\text{ox}} - E_{0-0}$ . NHE vs the vacuum level was set to 4.5 V.<sup>16</sup>

Cyclic voltammetry (CV) measurement was used to study the redox behavior of **TD1**, **TD2**, and **TD3** in CH<sub>2</sub>Cl<sub>2</sub> with a 100 mV s<sup>-1</sup> scan rate and calibrated against ferrocene (0.63 V vs. NHE),<sup>17</sup> using 0.1 M tetrabutylammonium hexafluorophosphate as the supporting electrolyte. The oxidation potential of the organic dyes was determined from the peak potentials by CV, and the oxidation potential ( $E_{\text{ox}}$ ) corresponded to the highest occupied molecular orbital (HOMO), while the lowest unoccupied molecular orbital (LUMO) could be calculated from  $E_{\text{ox}} - E_{0-0}$ . As shown in Table 1, these triazatruxene-based sensitizers show a first reversible oxidation wave at 0.91 (**TD1**), 0.90 (**TD2**), and 0.93 V (**TD3**), respectively. As a result, the ground-state oxidation potentials of the three dyes are higher than the redox potential of the iodide/triiodide redox couple (0.4 V vs. NHE) in all cases. On the other hand, the LUMO of these dyes (-1.12, -1.17, and -1.20 V vs. NHE, respectively) are also more negative than the conduction band of TiO<sub>2</sub> (-0.5 V vs. NHE). These values allow an effective electron injection into the conduction band (CB) of TiO<sub>2</sub> and ensure the regeneration of the oxidized form of the dyes in a DSSC.

To obtain deep insight into the molecular structure and frontier molecular orbitals of **TD1**, **TD2**, and **TD3**, the geometries of these dyes were optimized by density functional theory (DFT) calculations at the B3LYP/6-31G(d)

level. The electron distributions of the HOMO and LUMO of these dyes are shown in Figure 3. For the HOMO, the electron density is uniformly distributed along the triazatruxene unit and the  $\pi$ -spacer bridging unit, whereas the LUMO shows localized electron distributions though the cyanoacrylic acid and its adjacent  $\pi$ -spacer due to the intramolecular charge transfer along the  $\pi$ -conjugated skeleton. These electron distributions will therefore ensure efficient electron injection from the dye to the conduction band of TiO<sub>2</sub>.

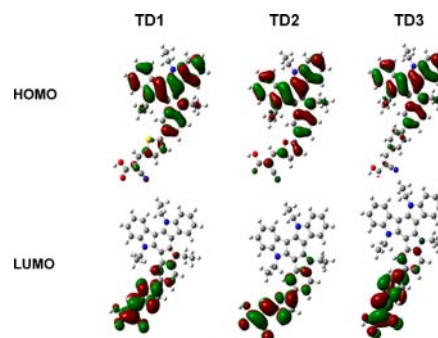


**Figure 3.** Electron distributions of the HOMO and LUMO of the dyes **TD1**, **TD2**, and **TD3**.

**Table 2.** Photovoltaic Performance of **TD1–3** and Reference **N719**<sup>a</sup>

dye	$V_{\text{oc}}$ /mV	$J_{\text{sc}}$ /mA cm <sup>-2</sup>	ff	PCE %
<b>TD1</b>	670	14.7	0.62	6.10
<b>TD2</b>	654	13.6	0.62	5.50
<b>TD3</b>	686	11.6	0.64	5.11
<b>N719</b>	734	16.9	0.63	7.82

<sup>a</sup> Active area is 0.16 cm<sup>2</sup>. Electrolyte is composed of 0.3 M 1,2-dimethyl-3-propylimidazolium iodide (DMPII), 0.1 M LiI, 0.05 M I<sub>2</sub>, and 0.5 M 4-*tert*-butyl pyridine in acetonitrile.

Liquid DSSCs were fabricated to test the photovoltaic performance of **TD1**, **TD2**, and **TD3**. (The method for the cell fabrication and photovoltaic characterization are described in the Supporting Information (SI).) The DSSC performance parameters of **TD1–3** and the standard **N719** dye are displayed in Table 2. The photocurrent density–voltage ( $J-V$ ) curves of these dyes are plotted in Figure 4. The DSSC performances of all the dyes are evaluated under AM 1.5 G irradiation at 100 mW cm<sup>-2</sup> with a 0.16 cm<sup>2</sup> active surface area. The solar cell based on **TD1** showed a power conversion efficiency (PCE) of 6.10%, with a short-circuit photocurrent density ( $J_{\text{sc}}$ ) of 14.7 mA cm<sup>-2</sup>, an open-circuit photovoltage ( $V_{\text{oc}}$ ) of 670 mV, and a fill factor (ff) of 0.62 under standard conditions. When the conjugating  $\pi$ -spacer thiophene was replaced by furan, the  $V_{\text{oc}}$  and  $J_{\text{sc}}$  of the resulting **TD2** ( $V_{\text{oc}}$ : 654 mV;  $J_{\text{sc}}$ : 13.6 mA cm<sup>-2</sup>) were both decreased. The solar cell based on **TD2** finally showed an efficiency of 5.50%, with a fill factor of 0.62. At the same

(15) Liu, J.; Numata, Y.; Qin, C.; Islam, A.; Yang, X.; Han, L. *Chem. Commun.* **2013**, 49, 7587.

(16) Gao, P.; Tsao, H. N.; Grätzel, M.; Nazeeruddin, M. K. *Org. Lett.* **2012**, 14, 4330.

(17) Liang, Y.; Peng, B.; Liang, J.; Tao, Z.; Chen, J. *Org. Lett.* **2010**, 12, 1204.

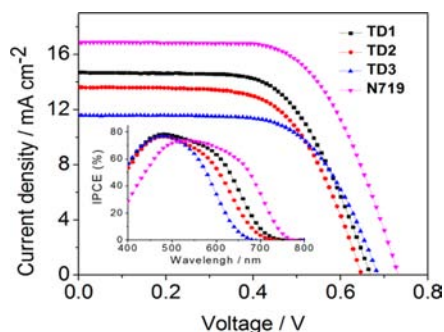


**Figure 4.** Photocurrent density–voltage ( $J$ – $V$ ) curves and the IPCE spectra (inset) of **TD1**–**3** and **N719**.

time, the solar cell based on **TD3** (with a benzene ring as the conjugating  $\pi$ -spacer;  $V_{oc}$ : 686 mV;  $J_{sc}$ : 11.6 mA cm<sup>−2</sup>) showed an efficiency of 5.11%, with a fill factor of 0.64. The best efficiency of **TD1** reached about 78% of the ruthenium dye **N719**-based standard cell fabricated and measured under the same conditions. To analyze the difference between the  $J_{sc}$  values, the incident photon-to-current conversion efficiencies (IPCEs) as a function of incident wavelength for DSSCs based on these dyes are plotted as the inset in Figure 4. As shown in IPCE spectra, the dyes **TD1**–**3** can all efficiently convert the light to photocurrents in the region from 400 to 700 nm. However, the onsets of the IPCE spectra for **TD1**–**3** are at 750, 730, and 690 nm, respectively, which are significantly broadened compared with those of their UV–vis absorption spectra in THF. The IPCE value changing tendency of these dyes is in accordance with their UV–vis absorption spectra in THF solutions. Moreover, the **TD1** based cell gave over 60% IPCE values from 410 to 610 nm with a maximum IPCE value of 78% at 480 nm, and its photocurrent signal is up to about 750 nm. The high IPCE value and broader absorption of **TD1** explained the high  $J_{sc}$  value from the  $J$ – $V$  measurement. The somewhat

higher efficiency observed for **TD1** is mainly due to the relatively larger  $J_{sc}$ .

Electrochemical impedance spectroscopy (EIS) is a powerful technique of characterizing the important interfacial charge transfer and carrier transportation process in DSSCs.<sup>18</sup> EIS Nyquist plots and Bode phase plots measured in the dark under forward bias (−0.65 V) are shown in Figure S1 (SI). The larger semicircle in the lower frequency range represents the interfacial charge transfer resistances ( $R_{ct}$ ) at the TiO<sub>2</sub>/dye/electrolyte interface.<sup>19</sup> The fitted  $R_{ct}$  increases in the order **TD2** (55  $\Omega$ ) < **TD1** (110  $\Omega$ ) < **TD3** (249  $\Omega$ ). This trend appears to be consistent with the values of open circuit voltage. A larger  $R_{ct}$  commonly indicates that the electron recombination in the devices is strongly reduced, thus resulting in a smaller dark current and a larger value of open-circuit photovoltage.<sup>20</sup> The electron lifetime ( $\tau$ ), another important parameter for DSSCs, could be extracted from the peak frequency ( $f$ ) at a lower frequency region in EIS Bode plots using  $\tau = 1/(2\pi f)$ .<sup>21</sup> In general, a longer electron lifetime corresponds to a larger value of  $V_{oc}$ . The electron lifetime ( $\tau$ ) was estimated to follow the trend **TD2** (16 ms) < **TD1** (32 ms) < **TD3** (47 ms), which is in good agreement with the above-mentioned result.

In conclusion, three new D– $\pi$ –A type organic sensitizers **TD1**, **TD2**, and **TD3** composed of a triazatruxene donor, a cyanoacrylic acid acceptor, and an aromatic  $\pi$ -bridge have been successfully designed and synthesized. All sensitizers have shown significant performance in dye-sensitized solar cells (over 5% power conversion efficiency), and the highest PCE value is up to 6.1% with a thiophene as the linker. The results demonstrate that the triazatruxene-based sensitizer can produce high photocurrent density and is a promising candidate in DSSCs. Further studies for triazatruxene-based sensitizers with higher efficiency through molecular modifications are ongoing in our laboratory.

**Acknowledgment.** The authors wish to thank the 973 Program (2011CB932502) and NSFC (Nos. 21172126 and 21272123) for their generous financial support.

**Supporting Information Available.** Detailed experimental procedures and characteristic data are provided. This material is available free of charge via the Internet at <http://pubs.acs.org>.

The authors declare no competing financial interest.

(18) Li, W.; Wu, Y.; Zhang, Q.; Tian, H.; Zhu, W. *ACS Appl. Mater. Interfaces* **2012**, *4*, 1822.

(19) van de Lagemaat, J.; Park, N.-G.; Frank, A. J. *J. Phys. Chem. B* **2000**, *104*, 2044.

(20) Hao, X.; Liang, M.; Cheng, X.; Pian, X.; Sun, Z.; Xue, S. *Org. Lett.* **2011**, *13*, 5424.

(21) Pei, K.; Wu, Y.; Wu, W.; Zhang, Q.; Chen, B.; Tian, H.; Zhu, W. *Chem.—Eur. J.* **2012**, *18*, 8190.